Scanning tunneling microscopy study of natural black arsenic

Xingfu Cai [1,2] Qi Wei [1] and Jiamin Xue [1,*]

[1] *School of Physical Science and Technology, ShanghaiTech University, Shanghai 201210, China*

[2] *University of Chinese Academy of Sciences, Beijing 100049, China*

(Received 14 July 2022; revised 3 September 2022; accepted 7 September 2022; published 19 September 2022)

Black arsenic (BAs) has emerged to be an interesting elemental layered material after graphite and black phosphorus (BP), which can be exfoliated to yield high-quality two-dimensional flakes. Transport measurements have revealed its strong in-plane anisotropy, giant Stark effect, and strong spin-orbital coupling, all resulting from its special electronic properties. On the other hand, previous synthetic analysis indicated that the pure BAs phase is unstable and could only be stabilized by a substantial percentage of impurities. Thus, a microscopic study of its structural and electronic properties is important for understanding this material. Here, we use scanning tunneling microscopy and spectroscopy assisted with first-principles calculations to investigate natural BAs at the atomic level. A puckered lattice structure like that of BP is measured. A bandgap of ∼0.29 eV is detected with the Fermi level located close to the conduction band. The most common defects form parallel stripes along a specific crystal direction and are shown to be the possible origin of the *n*-type doping in the natural BAs. These results provide valuable information for further study of BAs.

DOI: 10.1103/PhysRevB.106.125415

I. INTRODUCTION

Since the exfoliation of black phosphorus (BP) [1,2], the two-dimensional group-VA materials have sparked interest for their unique atomic structure and electronic properties [3]. The puckered lattice of BP results in a strong in-plane anisotropy [4–7]. For instance, the carrier mobility of monolayer BP along the armchair direction could reach 1000 cm^2/Vs at room temperature [1,8], which is about two times that along the zigzag direction [1,6–9]. As for the band structure, as-grown bulk BP is a *p*-type doped semiconductor with a direct bandgap of ∼0.38 eV [10–12]. Black arsenic (BAs), isomorphic to BP, has the same centrosymmetric lattice structure and even more intriguing electronic properties. The mobility of BAs shows enormous in-plane anisotropy. The hole Hall mobility along the armchair direction reaches an order of magnitude higher than that of the zigzag direction [13]. The valance band edge of BAs consists of three valleys close in energy, which may be tuned by an external electric field [14]. In addition, the element arsenic is heavier than phosphorus, so the spin-orbital coupling effect of BAs is much more remarkable, which produces electric-field controlled Landau level sequences in few-layer BAs [14].

Compared with BP, a special issue with BAs is its phase stability [15]. Unlike BP, which is the stable phase of phosphorus allotropes, BAs was calculated to be metastable and could only be stabilized by a high percentage of foreign atoms, e.g., 17% or more phosphorus was detected in synthesized BAs crystal [15]. However, recent transport studies are all based on the rare natural BAs mineral, arsenolamprite [13,14,16,17]. Its microscopic structural and electronic properties are thus important for the understanding of this interesting material. In this paper, we study the natural BAs crystals at the atomic level by scanning tunneling microscopy (STM) and spectroscopy (STS) assisted with density functional theory (DFT) calculations. The atomic structure of its basal plane is shown to be like that of BP, consisting of zigzag arsenic chains with no signature of high percentage of foreign atoms. The surface atoms are found to locate at two different heights, which cannot be reproduced by theoretical calculations and bulk x-ray diffraction (XRD) data. STS shows a bandgap of 0.29 eV with the Fermi level located close to the conduction band edge, indicating the *n*-type doping of this narrow-gap semiconductor. This doping could originate from the most common defects in BAs, which form parallel lines along the [111] direction. These results provide important basic information for natural BAs crystals and will benefit future study of this interesting material.

II. EXPERIMENTAL AND CALCULATIONAL METHODS

The BAs sample was cleaved from natural arsenolamprite under high vacuum $<5 \times 10^{-10}$ mbar. All STM and STS measurements were carried out at liquid helium temperature. DFT calculations were performed by the Vienna *Ab initio* Simulation Package (VASP) with Perdew-Burke-Ernzerhof generalized gradient approximation [18,19]. The first Brillouin zone was sampled using $10 \times 10 \times 12k$-meshes [20]. The energy cutoff was set as 500 eV for the whole calculations. In global geometry optimization of bulk BAs, the van der Waals interaction was performed by the optB88-vdw exchange functional [21]. The lattice constant and all atomic positions were allowed to relax until the force on each atom was <0.001 eV/Å.

*xuejm@shanghaitech.edu.cn

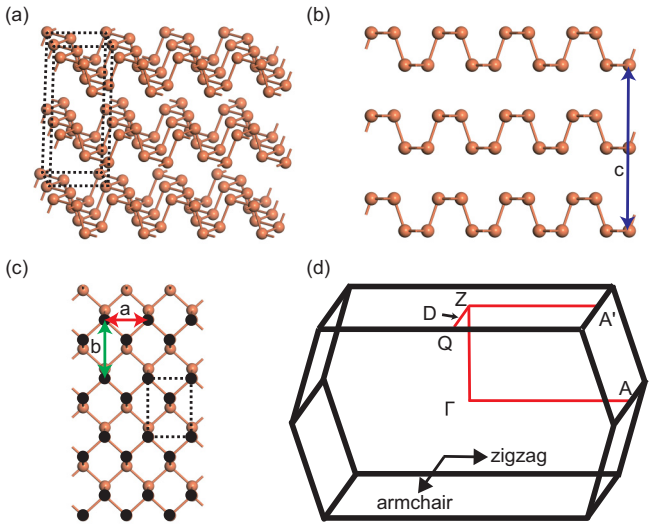

FIG. 1. (a) Perspective view of the black arsenic (BAs) crystal. The conventional unit cell is marked by the black dashed lines. (b) Puckered layer structure. Blue arrow indicates the lattice vector **c** of the conventional cell. (c) Top view of a monolayer BAs. The topmost atoms are colored in black, which are at the same height in bulk BAs determined by x-ray diffraction (XRD). The red (green) arrow along the zigzag (armchair) direction is the lattice vector **a** (**b**) of the surface unit cell. (d) Bulk BAs Brillouin zone and high-symmetry points.

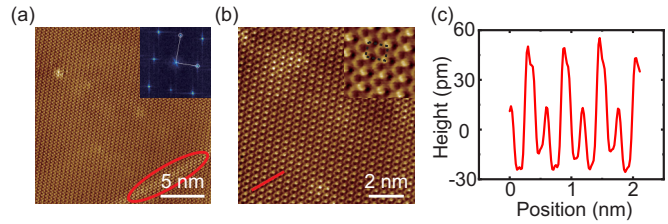

FIG. 2. (a) Scanning tunneling microscopy (STM) topography of black arsenic (BAs) surface at bias voltage $V = 0.7$ V and tunneling current $I = 70$ pA. The insert is the Fourier transformation of the main panel, which shows an orthorhombic lattice of the surface. (b) Zoom-in STM image obtained with $V = 0.7$ V, $I = 50$ pA showing the topmost atoms of the puckered layers. The insert is an enlarged STM topography of a 2×2 nm^2 area, showing the two different heights of atoms. (c) Line profile along the diagonal direction of the orthorhombic lattice [red line in (b)].

III. RESULTS

Like phosphorus, arsenic also has several allotropes [3]. Among them, the rhombohedral gray arsenic is the most stable and common phase [15], while the natural orthorhombic BAs has only been discovered at a few mining sites. Figure 1(a) shows the lattice structure derived from single-crystal XRD with the conventional unit cell indicated by the black dashed lines [22]. Neighboring layers are relatively displaced by half a lattice constant along the zigzag direction, so the lattice vector **c** [the blue arrow in Fig. 1(b)] consists of two monolayers. As illustrated in Fig. 1(b), bulk BAs is a puckered layered material under ambient pressure, like BP. The atoms are arranged as alternating valleys and ridges. Note that, in each layer, the atoms can be grouped into two planes, and the STM should detect the atoms in the topmost plane, which are shown in black in Fig. 1(c). The two-dimensional unit cell is a rectangle encircled by the black dashed lines. The red and green arrows point out the zigzag and armchair directions, respectively. The difference of atomic structure along the two directions of BAs indicates strong in-plane anisotropy of electronic properties. Figure 1(d) shows the first Brillouin zone corresponding to the primitive unit cell and high-symmetry paths where the calculated band edges are located. Line ZQ is along the armchair direction and line ZA' is along the zigzag direction.

In Fig. 2(a), a typical large-scale STM image shows the zigzag chains of BAs vividly. The insert Fourier transformation reveals the square lattice as expected in Fig. 1(c), from which the lattice constants a and b can be measured as 3.61 and 4.54 Å, respectively, in good agreement with the bulk XRD data in Table I [22]. A few scans contained step edges (not shown here) of height ~5.63 Å, corresponding to one layer of BAs. Some slight topography variations can be seen, especially a straight stripe (in the red oval) near the lower right corner in Fig. 2(a), but the lattice structure on the surface is continuous. These are the most commonly seen defects in BAs, presumably due to some arsenic atoms replaced by foreign elements, which will be discussed in more detail later, while in BP, the common defects are missing atoms which cause distinct dumbbell-shaped electron standing waves around them [11,12]. The percentage of the impurities in BAs can be roughly estimated by dividing the number of defect sites over the number of atoms in a scan, which is $1.50 \pm 0.15\%$ based on the analysis of seven scans, much lower than that of previously synthesized BAs [15]. The zoom-in image of Fig. 2(b) reveals the surface structure more clearly. Particularly, there is a visible height contrast of atoms in the zigzag chains [insert of Fig. 2(b)]. The line profile along the diagonal direction of the orthorhombic lattice [red line in Fig. 2(b)] is shown in Fig. 2(c). The height difference of atoms is ~33 pm, ~9% of the lattice constant, which was not found in the XRD data of bulk BAs crystals [22].

To simulate the surface atomic structure, a six-layer BAs slab model was built with a vacuum layer of 17 Å. The positions of atoms were allowed to relax until the force on each atom was <0.001 eV/Å. To simulate the possible surface geometry, two methods were used to optimize the BAs slab model. The first one is global atomic position optimization, which shows that the height difference of two types of atoms on the surface is ~0.002 Å. The other method is to fix the lowest two layers in the slab model with the XRD determined structure while optimizing the rest of the atomic positions [10]. However, the calculated height difference of the two

TABLE I. Lattice constants of BAs.

Measured by STM	Previous XRD data
$a = 3.61$ Å	$a = 3.65$ Å
$b = 4.54$ Å	$b = 4.47$ Å
$c = 11.26$ Å	$c = 11.00$ Å

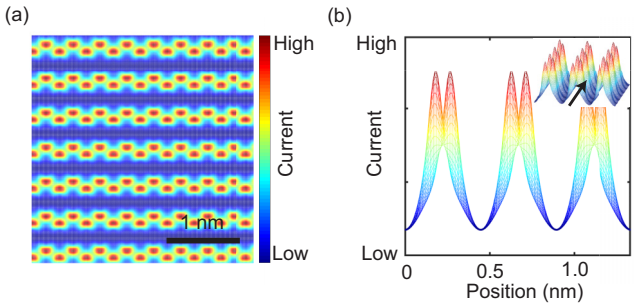

FIG. 3. (a) Simulated constant height scanning tunneling microscopy (STM) image of a six-layer black arsenic (BAs) slab at a bias voltage $V = 0.7$ V and a tip height of 1 nm. (b) Side view of the simulated STM image in (a) along the zigzag direction (as shown in the inset), indicating that all the atoms on the surface have the same height.

types of atoms on the surface was even smaller. Using the Tersoff approximation [23], a simulated constant-height STM image with the first optimization method is shown in Fig. 3(a), which corresponds to a scan with a bias voltage of $V = 0.7$ V and tip height of 1 nm. Different colors represent tunneling current which is positively correlated with the height measured in Fig. 2. All atoms on the surface have similar contrast. In Fig. 3(b), the side view of the simulated STM image in Fig. 3(a) along the zigzag direction (as shown in the inset) illustrates that there is no discernable height difference of the two inequivalent atoms. Hence, the surface atom relaxation cannot be captured by the DFT calculation. A similar feature of BP has been observed before with STM but with no good explanation [10].

After the structural analysis, the electronic properties are then examined. The STS in Fig. 4(a) (red curve) illustrates that BAs is a semiconductor with a narrow bandgap of 0.29 ± 0.01 eV (average and standard deviation of 15 curves), and the Fermi level resides within ~28 meV of the conduction band edge, which indicates that the natural BAs is an n-type doped semiconductor. In comparison, the STS of bulk BP [black curve in Fig. 4(a)] shows a slightly bigger bandgap of ~0.38 eV and p-type doping. These band features determine their transport properties. When fabricated into few-layer field-effect transistors, the narrow gaps render ambipolar behavior, with the back gate capable of tuning the carrier type continuously from electrons to holes [1,6,8]. Thanks to the

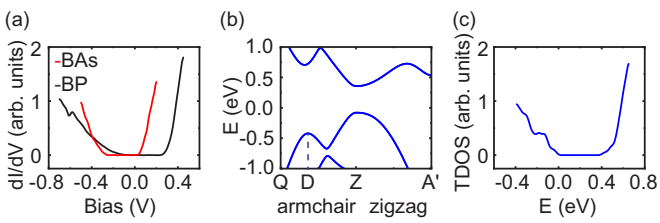

FIG. 4. (a) Red: dI/dV of bulk black arsenic (BAs). Black: dI/dV of bulk black phosphorus (BP). (b) Calculated bulk band structure of BAs along the high-symmetry lines. Z-Q is the armchair direction and Z-A' is the zigzag direction. (c) Calculated total density of states of bulk BAs.

TABLE II. Calculated effective masses of electrons and holes of bulk BAs and bulk BP.

	Carrier type	Zigzag direction	Armchair direction
BAs	Electron	$1.68\,m_0$	$0.21\,m_0$
	Hole	$1.40\,m_0$	$0.18\,m_0$
BP	Electron	$1.15\,m_0$	$0.12\,m_0$
	Hole	$0.71\,m_0$	$0.11\,m_0$

narrow gaps, electrical contacts can inject and extract both electrons and holes from the BAs and BP channels effectively, with no need to overcome large Schottky barriers that are common in other two-dimensional semiconductor devices. The smaller bandgap of BAs gives it an even more balanced electron-hole conductivity than that in BP [13,14].

DFT calculated energy bands in Fig. 4(b) show that bulk BAs is a direct bandgap semiconductor, and the band edges locate at the Z point. The gap size of 0.32 eV is in reasonable agreement with experimental results. In addition, there are two hole valleys approaching the valance band edge along the armchair direction at the two time-reversal symmetry-related D points. The energy difference between Z and D valleys is only 0.3 eV, which means that the valance band edge may be tuned from Z to D valley by external electrical field [14].

Moreover, both the BAs and BP STS curves have a steeper slope in the conduction band than that of the valance band, as shown in Fig. 4(a), which is a consequence of different density of states (DOS) at the band edges. The calculated total DOS of bulk black BAs in Fig. 4(c) reproduces well the STS measurement. For semiconductors, the band edge DOS difference can be captured by the analysis of effective masses, which are listed in Table II. The electron masses are heavier than the hole masses for both BAs and BP, indicating a larger DOS near the conduction band edge. Due to the strong structural anisotropy of the puckered lattice, the masses along the zigzag direction are larger than that along the armchair direction, which results in the strong transport anisotropy. This band structure is desirable for electronic devices which require both high current density and carrier mobility. Usually, high mobility in an isotropic semiconductor (such as GaAs) is achieved through small effective mass; hence, the band edge DOS and carrier density are low, leading to a compromised current density. In the strongly anisotropic BAs and BP, this dilemma could be resolved. High mobility can be realized by transport along the low effective mass direction, while the DOS can be provided by the weaker dispersion along the other direction.

Finally, we address the line defect and its electronic property. Scans on several samples all reveal straight stripes with different contrast compared with the atomic planes [one example is shown in Fig. 5(a)]. Their contrast could change with different scanning parameters [Fig. 5(b)], indicating that they are a result of DOS variation rather than topography features. The zoom-in over the stripe [inset of Fig. 5(a)] shows that the lattices are perfectly continuous, further supporting their DOS origin. Presumably arsenic atoms are replaced by foreign atoms along the stripes. The defects self-assembled into parallel lines along the [111] crystal direction. Previous

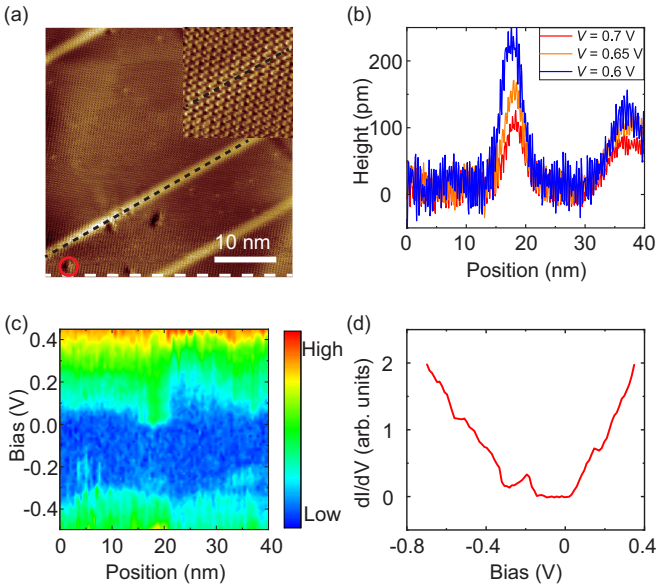

FIG. 5. (a) Topography of line defects at bias voltage $V = 0.7$ V and tunneling current $I = 70$ pA. The insert is an enlarged scan of a 5×5 nm^2 area along the black dashed line. (b) Topography across the line defect along the white dashed line in (a). The height varies with scanning parameters, indicating that it is caused by a difference of density of states (DOS) rather than physical height. (c) Scanning tunneling spectroscopy (STS) profile along the white dashed line at the bottom of (a). (d) STS at the point defect highlighted by the red circle in (a). An extra peak is seen in the gap near the valance band edge.

experiments have shown that, in some materials, defects could indeed form parallel one-dimensional structures and strongly affect the material property [24]. To study the electronic behavior of the defect, a dI/dV profile is taken along the white dashed line at the bottom of Fig. 5(a). Right on the stripe, the conduction band edge is clearly lower than that on the atomic plane and almost touches the Fermi level [Fig. 5(c)]. Similar results have been obtained on eight different stripes. Hence, these defects could be assigned as the possible source of the n-type doping in BAs. In addition to the line defects, some point defects are visible. One of them is highlighted by a red circle in Fig. 5(a), whose dI/dV spectrum is shown in Fig. 5(d). An extra peak is seen within the bandgap near the valance band edge. A similar peak near the valance band edge caused by point defects has been reported in BP [11], where this type of defects is abundant and could be the source of the p-type doping [11]. Since BAs is isomorphic to BP, the point defects presumably have similar electronic states.

IV. CONCLUSIONS

In this paper, we studied the structural and electronic properties of natural BAs crystal at the atomic level. The surface atomic structure is like that determined from the bulk XRD, except for a vertical relaxation. No significant content of impurities proposed in previous works about BAs is found. The bandgap of BAs is determined to be 0.29 ± 0.01 eV with n-type doping, which could be generated from an interesting type of line defects. These results provide information about the basic structural and electronic properties in BAs, which is important for further study and utilization of this material.

ACKNOWLEDGMENTS

The authors thank Prof. Qinglin Xia from Central South University, Prof. Hao Hu from Xi'an Jiaotong University, Prof. Wei Ji from Renmin University of China, and Dr. Shihao Zhang from ShanghaiTech for help with theoretical calculations. The authors thank Dr. Zhen Tian for the BP STS data. The authors appreciate the computational resources provided by Prof. Youqi Ke, Prof. Zhijun Ning, and the High Performance Computing (HPC) Platform at ShanghaiTech University. X.C. and J.X. are grateful for the financial support from ShanghaiTech University.

[1] L. Li, Y. Yu, G. J. Ye, Q. Ge, X. Ou, H. Wu, D. Feng, X. H. Chen, and Y. Zhang, Nat. Nanotechnol. **9**, 372 (2014).
[2] Y. Du, H. Liu, Y. Deng, and P. D. Ye, ACS Nano **8**, 10035 (2014).
[3] S. Zhang, S. Guo, Z. Chen, Y. Wang, H. Gao, J. Gomez-Herrero, P. Ares, F. Zamora, Z. Zhu, and H. Zeng, Chem. Soc. Rev. **47**, 982 (2018).
[4] J. Qiao, X. Kong, Z. X. Hu, F. Yang, and W. Ji, Nat. Commun. **5**, 4475 (2014).
[5] X. Ling, S. Huang, E. H. Hasdeo, L. Liang, W. M. Parkin, Y. Tatsumi, A. R. Nugraha, A. A. Puretzky, P. M. Das, B. G. Sumpter *et al.*, Nano Lett. **16**, 2260 (2016).
[6] F. Xia, H. Wang, and Y. Jia, Nat. Commun. **5**, 4458 (2014).
[7] X. Ling, H. Wang, S. Huang, F. Xia, and M. S. Dresselhaus, Proc. Natl. Acad. Sci. USA **112**, 4523 (2015).
[8] L. Kou, C. Chen, and S. C. Smith, J. Phys. Chem. Lett. **6**, 2794 (2015).
[9] H. Liu, Y. Du, Y. Deng, and P. D. Ye, Chem. Soc. Rev. **44**, 2732 (2015).
[10] C. D. Zhang, J. C. Lian, W. Yi, Y. H. Jiang, L. W. Liu, H. Hu, W. D. Xiao, S. X. Du, L. L. Sun, and H. J. Gao, J. Phys. Chem. C **113**, 18823 (2009).
[11] B. Kiraly, N. Hauptmann, A. N. Rudenko, M. I. Katsnelson, and A. A. Khajetoorians, Nano Lett. **17**, 3607 (2017).
[12] Z. Tian, Y. Gan, T. Zhang, B. Wang, H. Ji, Y. Feng, and J. Xue, Phys. Rev. B **100**, 085440 (2019).
[13] Y. Chen, C. Chen, R. Kealhofer, H. Liu, Z. Yuan, L. Jiang, J. Suh, J. Park, C. Ko, H. S. Choe *et al.*, Adv. Mater. **30**, e1800754 (2018).
[14] F. Sheng, C. Hua, M. Cheng, J. Hu, X. Sun, Q. Tao, H. Lu, Y. Lu, M. Zhong, K. Watanabe *et al.*, Nature (London) **593**, 56 (2021).
[15] O. Osters, T. Nilges, F. Bachhuber, F. Pielnhofer, R. Weihrich, M. Schoneich, and P. Schmidt, Angew. Chem. Int. Ed. **51**, 2994 (2012).

[16] M. Zhong, H. Meng, S. Liu, H. Yang, W. Shen, C. Hu, J. Yang, Z. Ren, B. Li, Y. Liu *et al.*, ACS Nano **15**, 1701 (2021).
[17] M. Zhong, Q. Xia, L. Pan, Y. Liu, Y. Chen, H. X. Deng, J. Li, and Z. Wei, Adv. Funct. Mater. **28**, 1802581 (2018).
[18] G. Kresse and J. Furthmuller, Phys. Rev. B **54**, 11169 (1996).
[19] J. P. Perdew, K. Burke, and M. Ernzerhof, Phys. Rev. Lett. **77**, 3865 (1996).
[20] V. Wang, N. Xu, J. C. Liu, G. Tang, and W. T. Geng, Comput. Phys. Commun. **267**, 108033 (2021).
[21] J. Klimes, D. R. Bowler, and A. Michaelides, J. Phys.: Condens. Matter **22**, 022201 (2010).
[22] P. M. Smith, A. J. Leadbetter, and A. J. Apling, Philos. Mag. **31**, 57 (1975).
[23] J. Tersoff and D. R. Hamann, Phys. Rev. B **31**, 805 (1985).
[24] B. Wang, W. Xia, S. Li, K. Wang, S. A. Yang, Y. Guo, and J. Xue, ACS Nano **15**, 7149 (2021).